PHYSICAL REVIEW E **88**, 060302(R) (2013)

Dynamical arrest in adhesive hard-sphere dispersions driven by rigidity percolation

Néstor E. Valadez-Pérez,[1,2] Yun Liu,[2,3] Aaron P. R. Eberle,[2] Norman J. Wagner,[3] and Ramón Castañeda-Priego[1,*]

[1]*División de Ciencias e Ingenierías, Campus León, Universidad de Guanajuato, Loma del Bosque 103, Lomas del Campestre, 37150 León, Guanajuato, Mexico*

[2]*The NIST Center for Neutron Research, National Institute of Standards and Technology, Gaithersburg, Maryland 20899-6100, USA*

[3]*Department of Chemical and Biomolecular Engineering, University of Delaware, Newark, Delaware 19716, USA*

(Received 23 June 2013; published 6 December 2013)

One major goal in condensed matter is identifying the physical mechanisms that lead to arrested states of matter, especially gels and glasses. The complex nature and microscopic details of each particular system are relevant. However, from both scientific and technological viewpoints, a general, consistent and unified definition is of paramount importance. Through Monte Carlo computer simulations of states identified in experiments, we demonstrate that dynamical arrest in adhesive hard-sphere dispersions is the result of rigidity percolation with coordination number $\langle n_b \rangle$ equal to 2.4. This corresponds to an established mechanism leading to mechanical transitions in network-forming materials [Phys. Rev. Lett. **54**, 2107 (1985)]. Our findings connect the concept of critical gel formation in colloidal suspensions with short-range attractive interactions to the universal concept of rigidity percolation. Furthermore, the bond, angular, and local distributions along the gelation line are explicitly studied in order to determine the topology of the structure at the critical gel state.

DOI: 10.1103/PhysRevE.88.060302 PACS number(s): 82.70.Dd, 64.70.pv, 64.75.Xc

Colloidal gels are observed in many fields, ranging from condensed matter physics to materials science and civil engineering (concrete is the prominent example), as well as biology and biotechnology and are at the heart of many consumer and food products [1,2]. However, due to the particular features of each system, we lack a general definition of gelation that allows us to understand, on one hand, the physical mechanisms that give rise to the formation of the arrested states of matter and, on the other hand, the route that connects a gel state with a glass transition in a continuous manner [1] (and vice versa).

Gels and glasses typically exhibit a solidlike behavior, such as yield stress, but show a liquidlike (disordered) structure [1,3]. There still exists a debate with respect to what makes a gel different from a glass [1,4]. One can find a large variety of properties or definitions that try to establish the differences of such out of equilibrium states. However, usually, a gel is viewed as a dilute suspension with a system-spanning network [1,3,5,6], whereas glasses are denser systems where caging is mainly responsible for dynamical arrest [7–9]. These features of gels and glasses depend on the interaction potential details. Therefore, an accurate knowledge of the interaction potential is needed to completely understand the mechanisms that give rise to a large diversity of arrested states. To reach this goal, well-controlled model systems that allow us to systematically tune the interparticle interaction are required [3,5,10].

The adhesive hard-sphere (AHS) system serves as a fundamental ground state in molecular and colloidal science for understanding the role of attractions in thermodynamics as well as nonequilibrium phenomena. A well-characterized, sterically stabilized, colloidal dispersion with adhesive interactions, controlled via temperature, has been recently developed to study the dynamical arrest [3,9]. Gelation in this system is defined using the classic Winter-Chambon rheological criterion [11]. A combination of small-amplitude oscillatory rheology and fiber-optic quasielastic light scattering is used to characterize the temperature at which dynamical arrest occurs. Small-angle neutron scattering (SANS) measurements of the structure of the dispersion at the gel temperature were carried out. This protocol allowed us to accurately determine the potential parameters, i.e., attraction range and well depth, in the liquid and the arrested states [3], and to evaluate the second virial coefficient [9]. The experimental error bars are less than 5% [9].

The main conclusions in [3,9] are that the dynamical arrest transition in systems with short-range attractions extends from the dilute particle concentration side of the liquid-vapor coexistence to above the critical point following predictions of dynamic percolation theory, until at sufficiently high particle concentrations ($\phi \geqslant 0.40$, where ϕ is the volume fraction) it subtends the predictions and joins the mode-coupling theory (MCT) prediction for the attractive-driven glass (ADG) [3,9].

The above scenario is expected to be universal for all systems composed of spherical Brownian particles that interact with short-range potentials as suggested by the Noro-Frenkel (NF) extended law of corresponding states [12], which condenses all the details of the interaction potential in a single parameter, namely, the reduced second virial coefficient, $B_2^*(T) \equiv B_2(T)/B_2^{\mathrm{HS}}$, where B_2^{HS} is the second virial coefficient of hard spheres. Although the NF extended law was originally proposed for the thermodynamic, i.e., equilibrium, properties, it has been recently shown that even dynamic properties of square-well (SW) fluids can be mapped onto a universal diagram in terms of the B_2 when the range of the potential is very short [13].

A common route to define a gel is through the concept of bonds [1]. Particles can form bonds with a certain probability and the lifetime of bonds makes possible a classification of gels; chemical gels are characterized by an irreversible bond formation, i.e., an infinite bond lifetime, whereas in a physical gel bonds can reversibly break and form when the particle

*ramoncp@fisica.ugto.mx

bonding is of the order of k_BT, i.e., the thermal energy, where k_B is the Boltzmann's constant and T the absolute temperature [1]. When the attraction between particles is below k_BT, the bond lifetime is small and no physical gelation occurs, but when the attraction overcomes the thermal energy, long-lived bonds appear that can lead to the formation of a gel state. Additionally, at sufficiently low densities the latter mechanism also gives rise to a gas-liquid phase separation [1,3,5]. However, although it is clear that the formation of bonds is the main driving force to form gels, the number of bonds needed to have a stable structure capable of supporting mechanical stresses in colloidal gels has not been established.

Here, we report Monte Carlo (MC) computer simulations of hard spheres with adhesive interactions along the experimentally determined dynamical arrest transition. We demonstrate that gelation in AHS dispersions is the result of rigidity percolation that occurs when the average number of bonds or coordination number takes the value of $\langle n_b \rangle = 2.4$. This value corresponds to that found within the context of mean-field transitions in random networks [14]. Hence, this common feature opens up the possibility of introducing a unified and general definition for gelation to the family of fluids that falls in the particular class of AHS dispersions. Further insight on the topology of the structures is gained by studying the local, bond, and angular distributions along the dynamical arrest line. We should stress that our findings make evident that phase separation cannot be considered as the universal mechanism for gelation, as suggested in depletion-based systems [5].

Within the context of network-forming materials, covalent glasses can be divided into two classes: those with low average coordination (polymeric glasses) and those with high average coordination (amorphous) [14,15]. This kind of glass consists of rigid and floppy regions, and undergoes a mechanical phase transition (not in the common sense of a transition between two phases) as the average coordination $\langle n_b \rangle$ is increased and rigidity percolates through the network [15]. He and Thorpe calculated that the glass transition takes place when $\langle n_b \rangle = 2.4$ [14]. In covalent glasses rigidity percolation leads to a permanent solid, whereas for physical bonds the solid persists on a time comparable with the bond lifetime.

The measured structure factor $S(q)$ in the AHS dispersion was modeled by assuming a short-range SW potential between colloids [3,9]. According to the experimental conditions, the range, in units of the particle diameter σ, is $\lambda = 1.01$ and the well depth ϵ was adjusted to accurately describe the structure probed through SANS experiments [3,9]. In the AHS limit, the strength of the interaction can be rewritten in terms of the $B_2^*(T)$ [3,9]. As shown by Noro and Frenkel, the specific choice of potential is not important as short-range attractions of less than ∼10% follow a law of corresponding states (see, e.g., Ref. [16], and references therein).

The functional form of the SW potential unambiguously defines when two particles are linked or form a bond; it happens when the separation between particles is less or equal to the interaction range λ. Another advantage of this potential is that the total potential energy can be directly expressed in terms of the average number of bonds, i.e., $\langle U \rangle = -2\langle n_b \rangle \epsilon$. We carry out MC simulations in the NVT ensemble with $N = 864$–4096 particles for those states above and below the arrested states within the concentration $0.11 < \phi < 0.48$ and the well-depth $-4.5k_BT < -\epsilon < -2.2k_BT$ intervals; the error bars obtained in the MC simulations are smaller than the symbol size used in the figures. For the sake of the discussion, we only show a few state points, particularly along the dynamical arrest line; however, the results of the full exploration will be reported elsewhere. The explicit details of the simulations can be found in Ref. [16].

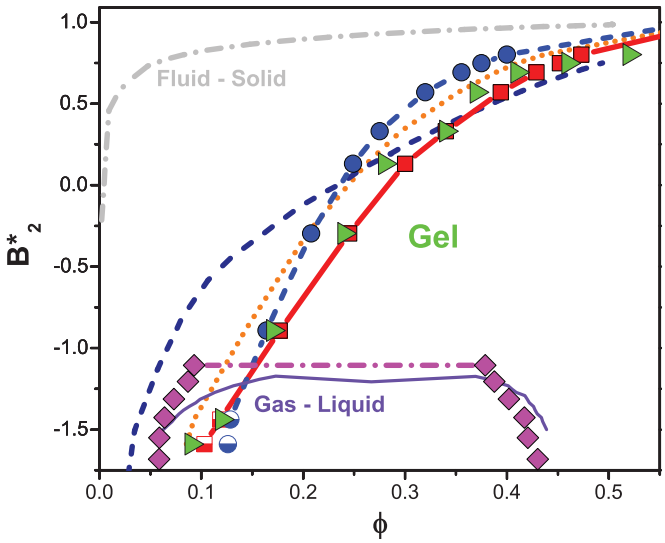

FIG. 1. (Color online) State diagram for the AHS system. The solid-dotted line is the fluid-solid coexistence as determined by the self-consistent phonon theory [17]. The solid line and diamonds are the gas-liquid coexistence regions for the AHS [18] and the SW fluid of range $\lambda = 1.01$ (this work), respectively. The dashed line is the MCT prediction of the AHS transition [19]. The connectivity between particles is represented by the percolation threshold (closed circles), whereas the dotted line and the line with closed squares represent those states with average coordination number values $\langle n_b \rangle = 2$ and $\langle n_b \rangle = 2.4$, respectively. Below the gas-liquid coexistence, these states are displayed with half-filled symbols. These are nonequilibrium states and are shown only to illustrate the fact that even below the spinodal they follow a similar trend as compared to the experimental curve, although they never reached the equilibrium within the simulation window. The right triangles are the experimentally determined dynamical arrest transition [3,9]. Continuous and broken lines between symbols are to guide the eye.

The state diagram for the AHS dispersion is presented in Fig. 1. One can appreciate that the arrested states and the gas-liquid phase separation are buried inside the fluid-solid coexistence [17], which confirms that both phenomena occur in the metastable region of the diagram. Particle polydispersity frustrates crystallization in the experiments. Moreover, in the NVT ensemble one is able to explore the metastable states in the computer simulations [16]; we only considered packing fractions that are below the spontaneous freezing, thus, polydispersity was not included in the simulations. The gas-liquid phase coexistences predicted by Miller and Frenkel [18] and that calculated for $\lambda = 1.01$ are plotted. We observe that both equilibrium diagrams are comparable. The dynamical arrest line, which corresponds to critical gel formation [11], obtained in experiments [3,9] is also shown, along with the MCT predictions [19] and the loci of states with a coordination number equal to 2 and 2.4.

At low concentrations, $\phi \lesssim 0.15$, gelation occurs inside the gas-liquid coexistence [3,5,9,10,20]. Below the binodal, percolation is congruent with gelation as observed in numerous studies [5,20]. The formation of a percolating network, where particles are linked by high energetic bonds ($\sim 4k_BT$), provides stability and can modify the elastic properties of the suspension. Above the critical B_2^*, at intermediate and high concentrations $0.15 < \phi \lesssim 0.45$, percolation is necessary but not sufficient for gelation [21], as can be observed by comparing the experiments with the exact percolation line computed by MC simulations. In our previous work, it was concluded that the experimentally determined gel line is closely approximated by the percolation theory calculated from the Percus-Yevick approximation [3]. This conclusion, however, is scrutinized more carefully here. We find that the experiments indicate a systematically stronger attraction is required for gelation than that for percolation.

At the highest concentrations (> 0.4), the attractive glass transition is driven by the balance between the attractive potential and the repulsion due to excluded volume effects. This balance may lead to a large variety of distinguishable nonbonded and bonded repulsive glassy states [8]. Particularly, Fig. 1 shows that the MCT predictions for the ADG converge to the experimental results at high concentrations $\phi > 0.40$, but at lower concentrations deviations are seen. This is not unexpected as the ADG transition is a consequence of a delicate competition between caging and attractions, and this structural arrangement is only possible at higher volume fractions where there are sufficient nearest neighbors (see [1] for further discussions of the limitations of the MCT theory). Therefore, strong localization of bonds must play an important role in the dynamical arrest transition below $\phi < 0.40$. Moreover, $\phi_c \sim 0.4$ has been identified as the crossover from gel to glass transitions [9]. Around this point the slope of B_2^* with ϕ changes significantly [9], signaling a transition from a fluid dominated by strong bonding to a fluid dominated by excluded volume interactions augmented by weak bonding.

Of importance in the state diagram are those states that have average coordination numbers 2 (dotted line) and 2.4 (closed squares). Interestingly, the curve for $\langle n_b \rangle = 2$ closely approximates the exact percolation threshold line, whereas the curve for $\langle n_b \rangle = 2.4$ agrees quantitatively with our experimental gelation line. According to the mean-field model for network-forming materials, a system with a coordination number or average bond value of 2 can be mechanically deformed [14]. On the other hand, He and Thorpe demonstrated that random networks undergo a transition to a solid network when the $\langle n_b \rangle = 2.4$ [14]. In order to make a straightforward comparison and analogy with the results reported in Ref. [14], the bond distribution for the AHS along the line $\langle n_b \rangle = 2.4$ is shown in Fig. 2. This is a nonsymmetric distribution with a long tail that indicates particles are coordinated preferably with two to five particles as is typical for transitions of random networks [14]. Furthermore, the distribution is nearly invariant along this iso-coordination number line despite the significant change in volume fraction. Thus, different state points (ϕ, B_2^*) with the same average bond value would imply that the topology of the structure responsible for the critical gel shares some similarities along the same iso-coordination number line.

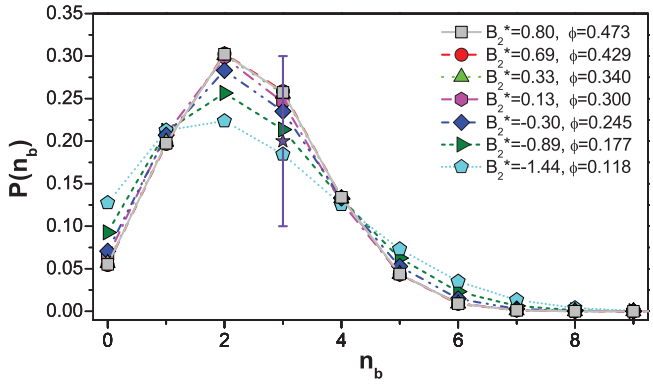

FIG. 2. (Color online) Bond distribution of the AHS system along the iso-coordination number curve $\langle n_b \rangle = 2.4$. The star with the error bar corresponds to the probability of finding a particle forming three bonds in model random networks [14].

He and Thorpe also calculated the probability distribution of having a coordination number of 3 in random networks [14]. This allows us a direct comparison with the probability of having particles forming three bonds in the AHS system along the iso-coordination curve $\langle n_b \rangle = 2.4$. Remarkably, the bond distributions (see Fig. 2) lie within the values reported in Ref. [14]. The same authors related the elastic transition in model random networks with the percolation of rigid regions, but in our simulations we cannot, strictly speaking, identify permanent rigidity. However, it is still possible to consider that particles forming four or more bonds are a reasonable representation of rigid regions. A visual representation of the particle distribution in real space is provided in Fig. 3. There, snapshots at two different volume fractions for three different iso-coordination curves are presented: $\langle n_b \rangle = 2$ (left), $\langle n_b \rangle = 2.4$ (middle), and $\langle n_b \rangle = 3$ (right). The left row, almost in the percolation state, exhibits isolated regions of high coordinated or bonded particles, while the middle and right rows display a percolation of highly coordinated particles. This

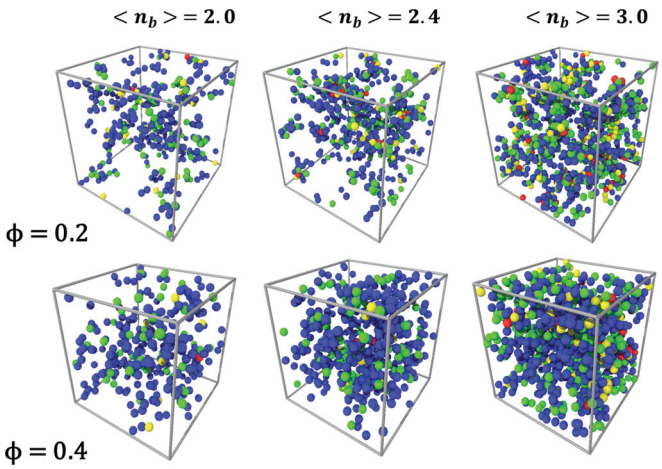

FIG. 3. (Color online) Snapshots of the AHS system at two different volume fractions for three different iso-coordination number curves: $\langle n_b \rangle = 2$ (left), $\langle n_b \rangle = 2.4$ (middle), and $\langle n_b \rangle = 3$ (right). Particles with four (blue), five (green), six (yellow), and seven or more (red) bonds are only displayed, which would correspond to rigid regions.

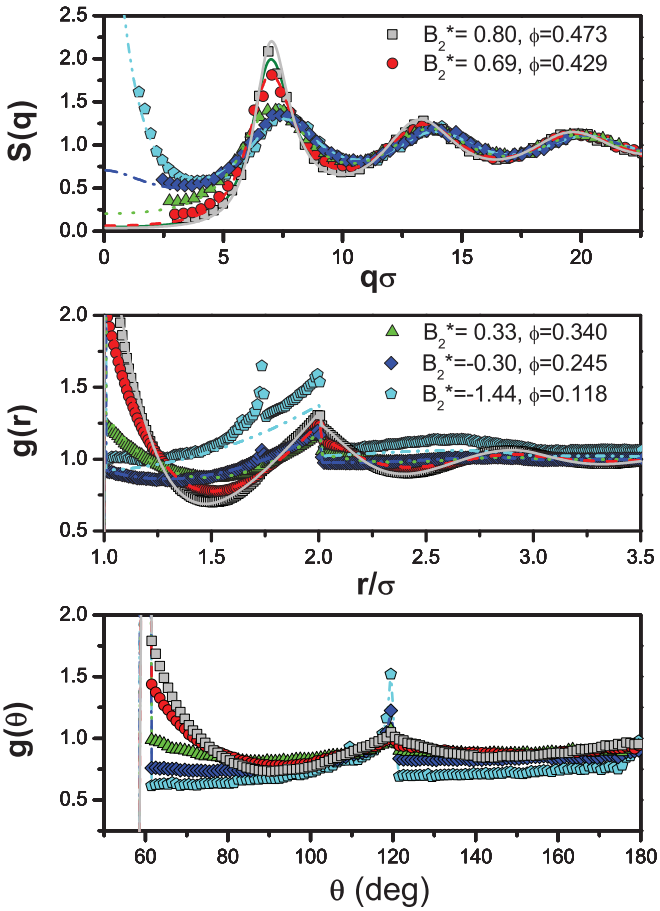

FIG. 4. (Color online) (a) Structure factor, (b) radial distribution function, and (c) angular bond distribution of the AHS system along the iso-coordination curve $\langle n_b \rangle = 2.4$. Symbols represent simulation data and solid lines are results of the Percus-Yevick approximation [3].

representation agrees with the physical picture suggested by He and Thorpe [14] and provides insight about the formation of compact structures during gelation.

To better understand the local arrangement of particles, the structure factor, the radial distribution function $g(r)$, and the angular distribution $g(\theta)$, along the iso-coordination curve $\langle n_b \rangle = 2.4$ are shown in Fig. 4. $g(\theta)$ represents the probability of finding three particles forming an angle θ, which is defined as the relative angle formed by three bonded particles [22]. The $S(q)$ exhibits a peak at $q\sigma \sim 2\pi$, which is related to the contact of particles and its height is always smaller than 2.85 (below the Hansen-Verlet's freezing criterion [3]). However, at low q and low densities the $S(q)$ shows an upturn that is associated with the formation of large scale particle correlations; the AHS system develops long-range correlations around and below the Boyle point ($B_2^* = 0$) [3,5,9]. At higher concentrations, such a correlation is absent as excluded volume effects dominate.

The behavior of the $g(r)$ along the gel line as shown in Fig. 4 can be explained as follows. At high concentrations, corresponding to high B_2^* values, the structure is similar to a hard-sphere liquid, i.e., weak bonds are present but particle correlations due to caging mechanics mainly contribute to the stability of the gel or attractive-driven glass structure. On the other hand, at low volume fractions, corresponding to low B_2^* values, strong bonds lead to correlations with specific angular distributions. In fact, peaks at $r/\sigma = \sqrt{3}$ are seen and can be associated with a plane trigonal particle distribution. The angular bond distribution $g(\theta)$ shows a maximum at 60°, which indicates that particles are arranged in an equilateral triangular structure. An additional peak at 120° is also found, and is linked to the peak found in the radial distribution at $r/\sigma = \sqrt{3}$. We do not observe the multiple peak angular distribution reported by Gao and Kilfoi for colloid-polymer mixtures [22]. This difference might be due to the more complex nature of a two-component system.

In conclusion, analysis of recent experiments of dynamical arrest of AHS nanoparticle dispersions by Monte Carlo simulations demonstrates that critical gel formation is the result of rigidity percolation of a dynamic network with an average value $\langle n_b \rangle = 2.4$. Thus, we show that dynamical arrest for AHS dispersions is driven by the same mechanism that leads to rigidity transition in network-forming materials. This discovery builds toward a consistent and unified definition of critical gel formation in systems with isotropic short-range attractions and it may have a very broad applicability for systems ranging from biological materials to cement. These findings can also enable quantitative prediction of important product properties for the manufacturing, fabrication, and processing of commercial products based on gels.

R.C.P. thanks Adrián Huerta for useful discussions on rigidity percolation. This work was financially supported by CONACyT (Grant No. 102339/2008) and NSF-CONACyT (project 147892/2011). The funding for A.P.R.E. was provided by the National Academy of Science through a National Research Council postdoctoral fellowship. This manuscript was prepared under cooperative agreement 70NANB7H6178 from NIST, U.S. Department of Commerce. The statements, findings, conclusions and recommendations are those of the author(s) and do not necessarily reflect the view of NIST or the U.S. Department of Commerce.

[1] E. Zaccarelli, J. Phys.: Condens. Matter **19**, 323101 (2007).
[2] M. Solomon and P. T. Spicer, Soft Matter **6**, 1391 (2010).
[3] A. P. R. Eberle, N. J. Wagner, and R. Castañeda-Priego, Phys. Rev. Lett. **106**, 105704 (2011).
[4] H. H. Winter, M. Siebenbürger, D. Hajnal, O. Henrich, M. Fuchs, and M. Ballauff, Rheo. Acta **48**, 747 (2009).
[5] P. J. Lu, E. Zaccarelli, F. Ciulla, A. B. Schofield, F. Sciortino, and D. A. Weitz, Nature (London) **453**, 499 (2008).
[6] M. Laurati, G. Petekidis, N. Koumakis, F. Cardinaux, A. B. Schofield, J. M. Brader, M. Fuchs, and S. U. Egelhaaf, J. Chem. Phys. **130**, 134907 (2009).

[7] F. Sciortino, Nat. Mater. **1**, 1476 (2002).
[8] E. Zaccarelli and W. C. K. Poon, Proc. Natl. Acad. Sci. **36**, 15203 (2009).
[9] A. P. R. Eberle, R. Castañeda-Priego, J. M. Kim, and N. J. Wagner, Langmuir **28**, 1866 (2012).
[10] J. M. Kim, J. Fang, A. P. R. Eberle, R. Castañeda-Priego, and N. J. Wagner, Phys. Rev. Lett. **110**, 208302 (2013).
[11] H. H. Winter and F. Chambon, J. Rheol. **30**, 367 (1986).
[12] M. G. Noro and D. Frenkel, J. Chem. Phys. **113**, 2941 (2000).
[13] G. Foffi, C. De Michele, F. Sciortino, and P. Tartaglia, Phys. Rev. Lett. **94**, 078301 (2005).
[14] H. He and M. F. Thorpe, Phys. Rev. Lett. **54**, 2107 (1985).
[15] M. F. Thorpe, J. Non-Cryst. Solids **57**, 355 (1983).
[16] N. E. Valadez-Pérez, A. L. Benavides, E. Schöll-Paschiner, and R. Castañeda-Priego, J. Chem. Phys. **137**, 084905 (2012).
[17] H. Shin and K. S. Schweizer, J. Chem. Phys. **138**, 084510 (2013).
[18] M. A. Miller and D. Frenkel, J. Chem. Phys. **121**, 535 (2004).
[19] M. A. Miller and D. Frenkel, J. Phys.: Condens. Matter **16**, S4901 (2004).
[20] F. Cardinaux, T. Gibaud, A. Stradner, and P. Schurtenberger, Phys. Rev. Lett. **99**, 118301 (2007).
[21] A. Coniglio, L. de Arcangelis, E. Del Gado, A. Fierro, and N. Sator, J. Phys.: Condens. Matter **16**, S4831 (2004).
[22] Y. Gao and M. Kilfoil, J. Phys.: Condens. Matter **16**, S5191 (2004).